HHS Public Access

Author manuscript

Clin Cancer Res. Author manuscript; available in PMC 2020 July 01.

Published in final edited form as:

Clin Cancer Res. 2020 January 01; 26(1): 290–300. doi:10.1158/1078-0432.CCR-19-1351.

Targeting EZH2 enhances antigen presentation, antitumor immunity and circumvents anti-PD-1 resistance in head and neck cancer

Liye Zhou[1], **Tenny Mudianto**[1], **Xiaojing Ma**[1,2], **Rachel Riley**[1], **Ravindra Uppaluri**[1,3]

[1]Department of Medical Oncology, Dana-Farber Cancer Institute, Boston, MA,

[2]School of Food and Biological Engineering, Hefei University of Technology, Hefei, Anhui, China,

[3]Department of Surgery/Otolaryngology, Brigham and Women's Hospital and Dana-Farber Cancer Institute, Boston, MA, USA

Abstract

Purpose: Anti-programmed death-1 (PD-1) receptor-based therapeutics improve survival in recurrent head and neck squamous cell carcinoma (HNSCC) patients but many do not benefit due to a low response rate. Herein, we identified EZH2 as a therapeutic target that enhanced tumor cell antigen presentation and subsequently sensitized resistant tumors to anti-PD-1 therapy.

Experimental design: EZH2 regulation of antigen presentation was defined using EZH2 inhibitors (GSK126 and EPZ6438) in human and mouse HNSCC cell lines. Mechanistic dissection of EZH2 in regulation of antigen presentation was investigated using flow cytometry, qRT-PCR, ELISA and chromatin-immunoprecipitation assays. EZH2 deficient cell lines were generated using CRISPR-CAS9. GSK126 and anti-PD-1 blocking antibody were used in testing combinatorial therapy in vivo.

Results: EZH2 expression was negatively correlated with antigen processing machinery (APM) pathway components in HNSCC TCGA datasets. EZH2 inhibition resulted in significant upregulation of MHC Class I expression in human and mouse human papillomavirus (HPV)-negative HNSCC lines in vitro and in mouse models in vivo. Enhanced antigen presentation on the tumor cells by EZH2 inhibitors or CRISPR mediated EZH2 deficiency, increased antigen specific CD8+ T cell proliferation, IFNγ production and tumor cell cytotoxicity. Mechanistically, EZH2 inhibition reduced the histone H3K27me3 modification on the β−2-microglobulin (B2M) promoter. Finally, in an anti-PD-1 resistant model of HNSCC, tumor growth was suppressed with combination therapy.

Conclusions: Our results demonstrated that targeting EZH2 enhanced antigen presentation and was able to circumvent anti-PD-1 resistance. Thus, combining EZH2 targeting with anti-PD-1 may increase therapeutic susceptibility in HNSCC.

Translational relevance

Corresponding Author: Ravindra Uppaluri, 45 Francis Street, Boston, MA, 02115. Phone: 617-632-3091; Fax: 617-394-2659; Ravindra_Uppaluri@DFCI.Harvard.edu.

Disclosures: RU has served on an advisory board for Merck.

Anti-PD-1 checkpoint inhibitor-based immunotherapies have shown clinical benefit in recurrent/metastatic HNSCC patients. However, new therapeutic strategies are needed to improve the low response rate. Herein, we identified EZH2 as a druggable target to enhance antigen presentation in HPV negative HNSCC. Targeting EZH2 sensitized tumor cells to T cell-mediated killing, increased antigen specific CD8+ T cell proliferation and IFNγ production in vitro. Mechanistic studies revealed that EZH2 modulated the histone H3K27me3 on the B2M promoter region. In an anti-PD-1 resistant model of HNSCC, combination EZH2 inhibition and anti-PD-1 suppressed tumor progression. Our results highlight a combinatorial therapeutic strategy of EZH2 inhibition and anti-PD-1 to enhance immunotherapeutic approaches in HNSCC patients.

Keywords

EZH2 inhibition; antigen presentation; anti-PD-1 resistance; combinatorial therapy; head and neck cancer

Introduction

Head and neck squamous cell carcinoma (HNSCC) is the sixth most common cancer worldwide (1). Patients with advanced human papillomavirus (HPV)-negative HNSCC have poor outcomes. Programmed cell death protein 1 (PD-1) checkpoint blockade with nivolumab or pembrolizumab has shown promising clinical outcomes in poor prognosis recurrent/metastatic HNSCC patients (2–6). However, the majority do not benefit with responses limited to 15–20% of patients. This resistance to immunotherapy is unexpected given the high mutational burden of cisplatin resistant tumors and the presence of immune infiltrates that together should predict better response rates (2–6). These findings lead to the question: can combination therapies directed at non-overlapping pathways improve outcomes of anti-PD-1 therapy in HNSCC?

Clinical responses to monoclonal antibodies blocking PD-1/PD-L1 signaling are based on the reversal of the dysfunctional exhausted state of tumor infiltrating T cells. Mechanistically, IFNγ production by tumor infiltrating T cells induces PD-L1 expression, among other downstream biologic changes, in the tumor microenvironment (7, 8). Deficiency of genes in the IFNγ signaling pathway or HLA class I have been shown to impair the efficacy of immunotherapy (9–11). Chan and colleagues reported that specific patient HLA class I genotypes are associated with response to immune checkpoint blockade (12). In HNSCC, dysfunctional HLA Class I antigen processing and presentation has been identified as a key factor contributing to tumor progression and immunotherapy resistance (13–15). Deficiency in the expression of HLA class I components, including B2M and specific HLA alleles, and antigen processing machinery have been correlated with poor prognosis of HNSCC (16, 17). Together, these observations suggest that approaches which enhance target tumor cell antigen presentation may improve the efficacy of anti-PD-1 therapy in HNSCC.

Enhancer of zeste homolog 2 (EZH2) is the methyltransferase subunit of the polycomb repressive complex 2 (PRC2) that catalyzes histone H3 methylation on lysine 27 (H3K27). This H3K27me3 histone modification can suppress chromatin accessibility and silence

downstream gene expression (18, 19). The role of EZH2 in different components of antitumor immunity has been investigated by several groups. Zou and colleagues reported the contribution of EZH2 in regulating T cell recruiting, Th1 chemokines, CXCL9 and CXCL10 in ovarian cancer cells. Consequently, combination therapy with EZH2 inhibition and adoptive T cell transfer resulted in better tumor growth suppression than either approach alone in ovarian tumor bearing mice (20, 21). In regulatory T cells (Tregs), disruption of EZH2 can enhance antitumor immunity by diminishing the suppressive activity of Tregs and enhancing T cell infiltration in the tumor (22, 23). Combining EZH2 inhibition with anti-CTLA4 resulted in a synergistic impact in mouse bladder carcinoma and melanoma models (23). Sommer, Boyman and colleagues reported the role of EZH2 in regulating a broad range of pathways impacting immunogenicity in melanoma (24). In addition, EZH2 is also involved in natural killer cell mediated tumor eradication in hepatocellular carcinoma by silencing the expression of NK group 2D (NKG2D) ligands (25). Very recently, diffuse large B-cell lymphoma showed a strong correlation between EHZ2 mutation enrichment and MHC class I and class II expression deficiency. EZH2 inhibition relieved suppression of NLRC5 and CIITA expression leading to increased expression but only in an EZH2 mutated background (26). However, in HNSCC, the specific role of EZH2 in modulating MHC Class I antigen presentation and T cell-mediated antitumor immunity has not been investigated.

In the present study, we hypothesized that inhibiting EZH2 function may improve the outcome of anti-PD-1 therapy by enhancing antigen presentation in HPV-negative HNSCC. Using both pharmacological inhibition and CRISPR-Cas9 mediated genome editing, we investigated the role of EZH2 in human HNSCC HLA Class I expression and also its role in antigen presentation and T cell-mediated killing in preclinical models. Extending these data to a novel anti-PD-1 therapy resistant preclinical model, we found that combinatorial therapy of GSK126, an EZH2 inhibitor, and anti-PD-1 showed significant tumor growth suppression compared to single agent therapy. Together, these data identify EZH2 as a potential therapeutic target in promoting antigen presentation and antitumor immunity in HNSCC.

Materials and methods

Cell lines and mice

Human HNSCC lines CAL-33, CAL-27, SCC-9, and SCC-25 were obtained from ATCC and maintained in the Dulbecco's Modified Eagle Medium/Nutrient Mixture F-12 (DMEM/F-12) + GlutaMAX™ media supplemented with 10% heat inactivated fetal bovine serum (FBS) and 100 U/ml penicillin streptomycin. Mouse oral squamous cell carcinoma models, MOC1-esc1 and MOC2, were maintained in IMDM/Hams-F12 (2:1) supplemented with 5% heat inactivated FBS, 100 U/ml penicillin streptomycin, 5 ng/ml EGF (Millipore), 400 ng/ml hydrocortisone (Sigma Aldrich), and 5 μg/ml insulin (Sigma Aldrich). Cell lines were routinely tested for mycoplasma and underwent short tandem repeat (STR) cell line authentication at the DFCI within 6 months of use. MOC1-esc1, an anti-PD-1 resistant line, is isogenic to the previously described MOC1 model (27). Derivation and further characterization will be described elsewhere (Zhou et al., in preparation). C57BL/6 mice (6-week-old, females) were from Taconic and OT-1 mice were purchased from Jackson Labs (C57BL/6-Tg (TcraTcrb)1100Mjb).

Reagents and antibodies

EPZ6438 and GSK126 were purchased from Selleckchem (S7128) and Chemietek (CT-GSK126), respectively. Recombinant human and mouse IFNγ were purchased from Peprotech (AF-300–02, AF-315–05). OVA (257–264) SIINFEKL peptide (AS-6-193-1) was purchased from AnaSpec. Primary antibodies against mouse EZH2 (4905, Cell signaling), β-actin (4967, Cell signaling), H3K27me3 (9733, Cell signaling), and Histone H3 (ab1791, Abcam) were used for western blot. Secondary antibody (IRDye® 800CW Goat anti-Rabbit IgG (H + L)) was purchased from LI-COR. EZH2 antibody (39901, Active Motif), H3K27me3 antibody (39055, Active Motif), and Rabbit IgG (15006, Sigma Aldrich) were used in the chromatin immunoprecipitation (ChIP) assay. For in vivo mouse studies, we used a rat anti-mouse monoclonal anti-PD-1(RMP1–14, BE0146) and a rat IgG2a isotype control (2A3, BE0089) from BioXCell.

Flow cytometry—Fluorophore conjugated antibodies specific for human HLA-A, B, C (W6/32, 311403), mouse CD45.2 (104, 109814), mouse H-2K^b (AF6–88.5, 116518), mouse PD-L1 (10F,9G2, 124312), mouse OVA-Kb (25-D1.16, 141603), and 7-AAD Viability Staining Solution (420403) from BioLegend were used in flow cytometry. Rat anti-mouse CD16/CD32 (2.4G2, 553142) was purchased from BD Biosciences. Mouse tumors were dissociated to single cell suspension with Tumor Dissociation Kit (130-096-730) and gentleMACS Dissociator (130-093-235) from Miltenyi Biotec. All flow cytometry analyses were performed on a MACSQuant analyzer 10 (Miltenyi) and interpreted using FlowJo10 (Treestar).

OT-1 T cell isolation, expansion, and co-culture killing assay

CD8+ T cells were isolated from OT-1 mouse splenocytes using CD8α+ T cell isolation Kit (130-104-075, Miltenyi Biotec). Isolated T cells were cultured in RPMI 1640, supplemented with 10% heat inactivated FBS, 20 mM HEPES (15630080, Gibco), 1mM sodium pyruvate (11360070, Gibco), 0.05mM 2-mercaptoethanol, 2 mM L-glutamine (G7513, Sigma), and 100 U/ml penicillin streptomycin. For activation, Dynabeads Mouse T-Activator CD3/CD28 (11456D, Thermo Fisher) were added to isolated T cells at a bead-to-cell ratio of 1:2. Recombinant mouse IL-2 (402-ML-020/CF, R&D systems) was added to a final concentration of 20 ng/ml on Day 1 after isolation. Medium supplemented with 20 ng/ml IL-2 was changed every 2 days. T cells were split every 2 days to keep an approximate cell density of 10^6 cells/ml. Activated OT-1 T cells were used for co-culture killing assay on Day 6–8 after isolation. For co-culture killing assays, mouse IFNγ (20 ng/ml) pre-stimulated tumor cells were pulsed with 0.02 nM of SIINFEKL peptide for 2 hours at 37 degrees. Activated OT-1 cells were counted and plated with washed tumor cells at indicated E:T ratios. After 24 hours of coculture, T cells were gently washed off using PBS. Surviving cells were harvested and stained with mouse CD45.2 antibodies to gate out residual T cells. Surviving tumor cells were counted using a MACSQuant Analyzer 10 (Miltenyi).

Immunoblotting

For the assessment of protein expression levels, RIPA buffer supplemented with protease inhibitor cocktail (11836153001, Sigma Aldrich) was used to homogenize cells. 50 μg of

total protein was separated on 4–12% SDS-PAGE gels (WG1403A, Invitrogen). Antibodies specific for mouse EZH2 (1:1000), β-actin (1:1000), H3K27me3 (1:1000), and total H3 (1:2000) were used for probing specific proteins. Secondary antibodies were then used to visualize specific proteins in a Li-Cor Odyssey imaging system.

Cell viability assay

Human or mouse cells (1500/ well) were plated in 96-well plates (3903, Corning) one day before starting drug treatment. Cells were treated with increasing concentrations of GSK126, EPZ6438, or vehicle (DMSO) for 72 hours. Cell viability was analyzed using CellTiter Glo-Luminescent cell viability assay (G7572, Promega). Luminescent signal was measured with an Infinite M200 Pro Multimode microplate reader (Tecan Life Science).

Quantitative real time PCR (qRT-PCR)

Total RNA was extracted from the cultured cells using RNeasy Mini Kit (74106, Qiagen). 1μg of extracted RNA was used for cDNA synthesis using High-Capacity cDNA Reverse Transcription Kit (4368814, Thermo Fisher Scientific) according to the manufacturer's instructions. TaqMan Real-time PCR Assays specific for mouse B2m (Mm00437762_m1), H2-K1 (Mm01612247_mH), Cxcl10 (Mm00445235_m1), Gapdh (Mm99999915_g1), human B2M (Hs00187842_m1), HLA-A (Hs01058806_g1), HLA-B (Hs00818803_g1), HLA-C (Hs00740298_g1), CXCL10 (Hs00171042_m1), and GAPDH (Hs02786624_g1) were purchased from Thermo Fisher and assays were performed on an ABI Step One Plus for quantifying gene expression levels. Data were analyzed using ΔΔCT method and normalized to GAPDH.

Chromatin Immunoprecipitation (ChIP) assay

ChIP assay was performed according per an Abcam protocol (https://www.abcam.com/protocols/cross-linking-chromatin-immunoprecipitation-x-chip-protocol). Briefly, tumor cells (10^7) were cross-linked with 1% formaldehyde and lysed with SDS lysis buffer. The chromatin extract was sonicated on a Covaris Ultrasonicator. For each precipitation, 5 μg of antibody was incubated with Dynabead Protein A/G (10001D and 10003D, Invitrogen) for 6 hours, and sequentially incubated with sonicated chromatin overnight. ChIP DNA was isolated and quantified. Quantitative PCR was performed using SYBR Green with the following primers. Primer sequences for B2M promoter region: Primer 1 Forward: 5'-GTCCGGATTGGCTGTGAGTT-3' and Reverse: 5'-GAGCCATGCTGACGACTGAA-3'; Primer 2 Forward: 5'-AGCTAGGAGACTGGTGACGA-3' and Reverse: 5'-AGCCATGCTGACGACTGAAG-3'.

In vivo studies

Female C57BL/6 mice (6-week old, Taconic) were housed in a pathogen-free animal facility and all experiments performed were approved by the Dana-Farber Cancer Institute IACUC. For tumor inoculation, MOC cells were harvested and washed extensively with cold endotoxin free PBS. Cells (10^6 MOC1-esc1, 10^5 MOC2) were injected subcutaneously into the right flank of each mouse in a volume of 150 μl. Anti-PD-1 therapy was performed by IP injections of anti-PD-1 (250 μg per mouse) or isotype control (250 μg per mouse) on

Day 3, 6, and 9 post-inoculation. GSK126 was dissolved in 20% Captisol (H107, Sigma Aldrich) and administered by IP injections 3 times a week from D6 post-inoculation. Tumor growth was monitored using a digital caliper twice weekly. Tumor volume was calculated using the formula $V= (W^2 \times L)/2$.

CRISPR/CAS9-mediated knock out of EZH2

LentiCas9-Blast (Addgene #52962) was co-transfected with pCMV-VSV-G and psPAX2 into HEK293T cells for lentivirus production using TransIT-293 (MIR2700, Mirus Bio). Virus in the media was collected 48 hours after transfection and MOC1-esc1 cells were transduced for 48 hours and then subjected to Blasticidin (4 μg/ml) selection for 4 days. Pooled MOC1-esc1-cas9 cells were single cell sorted in 96-well cell culture plate to generate single clones. Cas9 editing efficiency of each clone was tested by the assessing the knock out efficiency of B2M sgRNA expressing lentivirus transduced cells. H2-K^b class I cell surface expression levels were determined by flow cytometry as a readout of Cas9 efficiency (not shown). Clone #2 and #3 with high editing efficiency were transduced with lentivirus expressing specific gRNAs targeting EZH2 or ROSA26, respectively. The sequences of specific sgRNAs are listed below.

EZH2-g1-oligo1: CACCGTATCGTAGTAAGTACCAATG

EZH2-g1-oligo2: AAACCATTGGTACTTACTACGATAC

EZH2-g2-oligo1: CACCGAGAGTACATTATAGGCACCG

EZH2-g2-oligo2: AAACCGGTGCCTATAATGTACTCTC

ROSA26-oligo1: CACCGCAATCAGCGGAGGCTGCCG

ROSA26-oligo2: AAACCGGCAGCCTCCGCTGATTGC

T cell proliferation assay

Naïve CD8+ T cells isolated from OT-1 mouse splenocytes were stained with CFSE cell division tracker kit (423801, BioLegend) at a final concentration of 5 μM in PBS supplemented with 5% heat inactivated FBS for 3 mins in the dark at room temperature. After staining, cells were washed 3 times in PBS with 5% FBS. IFNγ pre-stimulated tumor cells were plated with CFSE labeled T cells at an E:T ratio of 10:1. After 72 hours co-culture, media were harvested for IFNγ ELISA. CD8+ T cells proliferation measured by CFSE-dilution was determined using flow cytometry.

TCGA data set analysis—Data for HNSCC and lung SCC patients from TCGA was obtained from cBioPortal. HPV status of patients was obtained from a PanCancer Atlas study (28). Gene expression correlations between EZH2 and molecules involved in antigen presentation machinery were assessed by Spearman’s coefficient.

Mouse IFNγ ELISA:

IFNγ levels in the media from T cell proliferation coculture experiments were measured with the Mouse IFN-gamma DuoSet ELISA (DY485, R&D Systems) according to the manufacturer's instructions.

Statistical analysis

Data are plotted as the mean ± SD or mean ± SEM as indicated in specific experiments. The statistical significance was determined by student's *t*-test, one-way ANOVA and 2-way ANOVA using GraphPad Prism. Significance differences $p<0.05$, 0.01, 0.001 were symbolized as *, **, and ***, respectively.

Results

EZH2 expression is negatively correlated with major MHC class I antigen presentation molecules

As antigen presentation defects have been identified as a common feature in HNSCCs, we sought to identify the relationship between EZH2 expression and antigen presentation pathway components. Analysis of 522 HNSCC HPV-negative tumors from TCGA (28) showed a significant inverse correlation between the EZH2 expression levels and major MHC class I antigen presentation molecules, including β2M, HLA-A, HLA-B, HLA-C, and HLA-E (Figure 1), highlighting a potential regulatory function of EZH2 on antigen presentation in HNSCC. Interestingly, this negative correlation was also seen in 483 HPV negative lung squamous cell carcinomas (Supplementary Figure 1).

EZH2 inhibition promotes antigen presentation and Th1-type chemokine expression in cell line models of human HNSCC

To test the hypothesis that targeting EZH2 could promote antigen presentation in HNSCC, we used two highly selective EZH2 inhibitors, GSK126 and EPZ6438 (22, 29, 30). Human HNSCC cell lines (CAL27, CAL33, SCC25, and SCC9) were treated with increasing concentrations of GSK126 or EPZ6438 to test the impact of EZH2 inhibition on cell viability. Based on the various sensitivities of these cell lines to EZH2 inhibitors, we selected the 10 μM concentration for both GSK126 and EPZ6438, at which neither inhibitor showed significant cell growth inhibition (Figure 2A). While GSK126 increased IFNγ induced HLA expression in 3 of 4 lines tested, EPZ6438 increased both basal and IFNγ induced HLA cell surface expression levels compared with DMSO control in all cell lines (Figure 2B). Given the known function of EZH2 as a methyltransferase that silences target genes, we quantified the mRNA expression changes of MHC class I antigen presentation genes, including B2M, HLA-A, HLA-B, and HLA-C after treatment with EZH2 inhibitors. Despite different sensitivities to EZH2 inhibition, major class I antigen presentation genes were upregulated by at least one EZH2 inhibitor under either basal, or exogenous IFNγ stimulated conditions, or both in all tested cell lines (Figure 2C and Supplementary Figure 2). Therefore, EZH2 regulated mRNA levels of antigen presentation genes. Consistent with findings in ovarian cancer (20), we also observed a significant induction of CXCL10 expression in EZH2 inhibitor treated cells compared with DMSO control that was

dramatically enhanced in combination with IFNγ (Figure 2C). Therefore, EZH2 inhibition influenced MHC class I expression and CXCL10 expression in human HNSCC lines.

EZH2 inhibition upregulated MHC class I antigen presentation in anti-PD-1 resistant mouse HNSCC cells

Aiming at reversing immunotherapy resistance in HNSCC, we tested the effect EZH2 inhibition in MOC1-esc1, a syngeneic anti-PD-1 resistant mouse model. When assayed for impact on cell viability assay, significant cytotoxicity in MOC1-esc1 was not seen with either EZH2 inhibitors at the 10 μM dose (Figure 3A). We then used GSK126 or EPZ6438 to determine the effect of EZH2 inhibition on antigen presentation in MOC1-esc1. Consistent with the data in human HNSCC, either treatment significantly upregulated MHC class I cell surface protein levels in combination with IFNγ (Figure 3B, C). To confirm that the role of EZH2 in antigen presentation modulation was not model specific, we performed similar experiments using MOC2, another immunotherapy resistant mouse HNSCC model. Consistent with the results in MOC1-esc1, EZH2 inhibitor treated MOC2 cells showed enhanced MHC class I expression (Figure 3C). To assess whether this increased expression also resulted in increased antigen presentation, we assessed levels of MHC class I-bound SIINFEKL. EZH2 inhibition also increased the presentation of SIINFEKL peptide by H2-K^b on the MOC1-esc1 and MOC2 cell surface confirming the functional upregulation of antigen presentation (Figure 3D). Together, these data showed that EZH2 inhibition increased antigen presentation in anti-PD-1 resistant HNSCC cells.

Pharmacological inhibition and genetic ablation of EZH2 in tumor cells enhance T cell-mediated killing

Next, we asked whether the EZH2 inhibition based enhanced MHC class I antigen presentation sensitized tumor cells to T cell-mediated killing. Note that in addition to pharmacological targeting and to further study the role of EZH2 in T cell / tumor cell interactions, we generated CRISPR-CAS9 genetically deleted EZH2 MOC1-esc1. We used 2 independent clones of CAS9 expressing MOC1-esc1 to knock out EZH2 with 2 different single guide RNAs (sgRNAs) to rule out clone specific or off-target effects. Immunoblotting for EZH2 was performed and showed attenuated EZH2 expression relative to ROSA26 control targeted lines (Figure 4A). We performed a 2-D co-culture assay using OT-1 CD8+ T cells that were *in vitro* activated and expanded with SIINFEKL peptide antigen pulsed tumor cells as targets. GSK126 or EPZ6438 treatment sensitized MOC1-esc1 cells to T cell-mediated killing (Figure 4B). Genetic ablation of EZH2 dramatically sensitized tumor cells to T cell-mediated killing in both clones in comparison with their parental lines and ROSA26 targeting controls (Figure 4B and Supplementary Figure 6). Consistent with the inhibitor treatment experiment results, loss of EZH2 significantly increased MHC class I cell surface expression levels which again were enhanced in combination with IFNγ without impacting PD-L1 (Figure 4C, D), indicating the specificity of this regulation on antigen presentation. Therefore, targeting of EZH2 sensitized tumor cells to T cell-mediated killing.

EZH2 represses antigen presentation by regulating the enrichment of H3K27me3 on the B2M promoter

To start to define the mechanism of EZH2 regulation of antigen presentation, we tested H3K27me3 levels in GSK126 or EPZ6438 treated cells. As expected, inhibition of EZH2 resulted in dramatic decrease of global H3K27me3 levels, without affecting the protein expression levels of EZH2 (Figure 5A). In addition, the mRNA levels of both B2M and H2-K1 were significantly upregulated by EZH2 inhibition (Figure 5B), suggesting that the regulation of EZH2 on antigen presentation is conserved between human and mouse (Figure 2B, C and Supplementary Figure 2). Interestingly, CXCL10 expression was not induced by EZH2 inhibition in this mouse model (Figure 5B).

To test the hypothesis that EZH2 regulates H3K27me3 occupancy on the promoter region of B2M, MOC1-esc1 cells were treated with EPZ6438 or DMSO and subjected to chromatin immunoprecipitation (ChIP) with antibodies against EZH2, H3K27me3, or IgG control. To test the occupancy of EZH2 and H3K27me3 modification on B2M promoter, DNA samples from ChIP were quantified using 2 independent primers specific for B2M promoter region. The results of ChIP assay followed by quantitative PCR showed that EPZ6438 treatment did not affect the binding of EZH2 on B2M promoter region (Figure 5C), which is in agreement with the mode of action of EPZ6438 as an S-adenosyl-I-methionine (SAM)-competitive inhibitor. Importantly, EPZ6438 treatment significantly reduced H3K27me3 enrichment on the B2M promoter region (Figure 5D).

Combinatorial therapy of GSK126 and anti-PD-1 suppresses MOC1-esc1 tumor progression *in vivo*

Next, we asked whether the enhanced antigen presentation in EZH2 deficient tumor cells can promote the function of antigen specific T cells. To answer this question, we analyzed CD8+ T cell proliferation and IFNγ production after coculture of SIINFEKL peptide pulsed tumor cells with naïve OT-1 T cells. These data show that both T cell proliferation and IFNγ production were significantly higher in EZH2 deficient tumor cells compared with ROSA26 control (Figure 6A, B, C). To investigate whether EZH2 inhibitor can improve the outcome of anti-PD-1 therapy, we used resistant MOC1-esc1 to assess the effect of combination therapy. MOC1-esc1 tumor growth in immunocompetent wild type mice was significantly attenuated by the combination of GSK126 (50 mg/kg) and anti-PD-1 but not by either agent alone (Figure 6E). To test the role of EZH2 inhibition in modulating antigen presentation of tumor cells in vivo, we analyzed the tumor samples with these treatment conditions (Figure 6F, G). Tumor cell MHC class I cell surface expression levels were increased by GSK126 monotherapy compared to the control group (Figure 6F). Similarly, anti-PD-1 monotherapy also increased the MHC class I level compared to control (Figure 6F). Interestingly, the combination of GSK126 and anti-PD-1 resulted in an additive increase of MHC class I (Figure 6F). Total CD45+ immune infiltration in the tumors was not affected by either monotherapy or combinatorial therapy (Figure 6G, Supplementary Figure 8). In summary, enhanced antigen presentation induced by targeting of EZH2 promoted proliferation and IFNγ production of antigen specific T cells and combination therapy of GSK126 and anti-PD-1 resulted in attenuation of tumor progression in an anti-PD-1 resistant mouse model of HNSCC.

In addition, as significant numbers of patients are resistant to immunotherapy due to poor immune infiltration, we asked whether the efficacy of GSK126 and anti-PD-1 combinatorial therapy requires pre-existing immune infiltration in tumors. We next assessed for combination therapy impact in the MOC2 model that displays an immune “desert” phenotype with negligible T cell infiltration and aggressive in vivo growth (31). Consistent with previous data (31), MOC2 tumors are resistant to anti-PD-1 treatment (Figure 6H). Neither GSK126 monotherapy nor the combination of GSK126 and anti-PD-1 suppressed tumor growth (Figure 6H). Although the growth phenotype was not altered, we assayed for in vivo MOC2 tumor cell Class I expression with different treatments. Neither the control nor the monotherapy groups displayed alteration in surface Class I expression. However, consistent with our observation in MOC1esc1 tumors, the combination group induced a significant higher MHC Class I on tumor cells in vivo. As for MOC1-esc1, there was minimal impact on CD45+ T cell infiltration. Therefore, EZH2 inhibition and anti-PD-1 combinatorial therapy upregulates tumor cell MHC Class I expression in vivo, while the therapeutic efficacy may require pre-existing immune infiltration.

Discussion

In order to define approaches to improve outcomes of anti-PD-1 therapy in HNSCCs, we identified that targeting the histone methyltransferase EZH2 enhanced antigen presentation in both human and mouse HNSCC lines. Mechanistic studies revealed that EZH2 inhibition decreased the enrichment of H3K27me3 on the promoter region of B2M. The enhanced antigen presentation induced by targeting EZH2 sensitized tumor cells to T cell-mediated killing, resulted in higher T cell proliferation and IFNγ production *in vitro*. These findings translated to a synergistic impact of combination GSK126 and anti-PD-1 in attenuating the tumor progression of an anti-PD-1 resistant model of HNSCC and showed that EZH2 inhibition can enhance tumor cell Class I expression in vivo including in highly resistant models. Our data define EZH2 as a therapeutic target to improve the outcome of anti-PD-1 therapy in HNSCC.

EZH2 inhibition has been proposed as a therapeutic strategy in cancers with frequent gain of function mutation or over-expression of EZH2, including melanoma, ovarian cancer, and lymphoma to induce apoptotic cell death (32–34). In HNSCC, overexpression of EZH2 has been correlated with poor prognosis, recurrence, and lymph node metastasis in HNSCC (35–37). Saunders et al. reported that targeting EZH2 in HNSCC attenuated tumor growth by inducing differentiation gene expression via modulating H3K27me3 occupancy on the promoter regions of genes involved in squamous differentiation (38). To test the effect of EZH2 inhibition on human HNSCC tumor progression, Cal27 was implanted in immunocompromised NOD/SCID mice, in which setting the interaction between tumor cells and host immunity was eliminated to support the human tumor growth in mice (38). These previous studies highlighted EZH2 inhibition as a potential therapeutic target in HNSCC by modulating epigenetic silencing of genes involved in tumor progression. In our study, we first demonstrated the effect of EZH2 inhibition on increasing antigen presentation is conserved in human and mouse HNSCC lines. Subsequently, a syngeneic mouse model was used to investigate the *in vivo* therapeutic potential of EZH2 inhibition independent from direct cytotoxicity of EZH2 on tumor cells. Thus, the present study provides a new line of

evidence in support of EZH2 inhibition as a new combination immunotherapy target in promoting HNSCC antitumor immunity to overcome checkpoint blockade resistance.

Consistent with other studies, inhibition of EZH2 significantly induced the expression of CXCL10 in human HNSCC lines (Figure 2C)(20). CXCL10 is a Th1-chemokine CXCL10 that is a key ligand regulating T cell trafficking into the tumor microenvironment through CXCR3 (39) (40). However, CXCL10 expression was not increased by EZH2 inhibition in the HNSCC mouse model (Figure 5B), suggesting the regulation of CXCL10 by EZH2 is not conserved in human and mouse models used in this study. Although speculative, this suggests that in human HNSCC, the effect of EZH2 inhibition on antitumor immunity might include enhanced antigen presentation and additionally, higher immune infiltration in tumors.

One limitation of this study is the lack of well-defined endogenous antigen and antigen specific T cells in the MOC1-esc1 HNSCC model. Therefore, we employed a commonly used model antigen, SIINFEKL peptide from ovalbumin, and OT-1 mouse derived antigen specific T cells for *in vitro* studies (41). Supporting the use of this approach, CRISPR-CAS9 knock out of B2M or PD-L1 in MOC1-esc1 resulted in resistance or sensitivity to T cell-mediated killing, respectively (data not shown). Therefore, this 2-D coculture system retained the relevant function of EZH2 in T cell recognition to tumor cells. Additionally, as EZH2 impacts a broad range of pathways in vivo, dissecting the specific immune contribution will require further studies. Our work supports that EZH2 has the capacity to directly regulate tumor cell Class I in vitro and that inhibition in vivo results in a similar end result of enhanced Class I expression. Further mechanistic dissection of in vivo antigen presentation is required.

Others have studied the contribution of EZH2 in augmenting tumor immunogenicity including antigen presentation regulation in melanoma and lymphoma, respectively (24, 26). Our study focused on HNSCCs and defined further details of antigen presentation regulation. Differences in HNSCC include that the frequency of EZH2 overexpression in HNSCC is relatively low compared with that in cutaneous melanoma, lymphoma, and ovarian cancers. In addition, there are no EZH2 gain-of-function mutations identified in HNSCC (19). Therefore, the sensitivity of HNSCC to EZH2 inhibition induced apoptosis may be relatively low. The function of EZH2 inhibition in promoting antigen presentation thus identifies a disease-specific contextual opportunity in which to consider EZH2 inhibitor as an immunotherapy agent in HNSCC.

Interestingly, the inverse correlation of EZH2 and MHC class I antigen presentation molecule expression levels in HNSCC TGCA dataset is also found in lung squamous cell carcinoma, suggesting the function of EZH2 in regulating antigen presentation may be conserved in squamous cell carcinomas from other tissues. Based on our results, we propose that combination EZH2 inhibition with anti-PD-1 therapy may be beneficial for HNSCC patients. Studies using different EZH2 inhibitors and additional HNSCC preclinical models are needed to further confirm our findings. In addition, the effect of EZH2 in regulating antigen presentation in professional antigen presentation cells (APC), such as macrophages and dendritic cells, also requires further investigation.

Supplementary Material

Refer to Web version on PubMed Central for supplementary material.

Acknowledgements:

This study was supported by the NIH/NIDCR (DE024403 and DE027736) to R. Uppaluri. We thank Drs. Zhong Wu and Deli Hong for technical assistance with CHIP.

Funding: Supported by NIH/NIDCR R01DE024403 and R01 DE027736

References

1. Jemal A, Bray F, Center MM, Ferlay J, Ward E, and Forman D. Global cancer statistics. CA Cancer J Clin. 2011;61(2):69–90. [PubMed: 21296855]
2. de Ruiter EJ, Ooft ML, Devriese LA, and Willems SM. The prognostic role of tumor infiltrating T-lymphocytes in squamous cell carcinoma of the head and neck: A systematic review and meta-analysis. Oncoimmunology. 2017;6(11):e1356148. [PubMed: 29147608]
3. Feng Z, Bethmann D, Kappler M, Ballesteros-Merino C, Eckert A, Bell RB, et al. Multiparametric immune profiling in HPV- oral squamous cell cancer. JCI Insight. 2017;2(14).
4. Hanna GJ, Liu H, Jones RE, Bacay AF, Lizotte PH, Ivanova EV, et al. Defining an inflamed tumor immunophenotype in recurrent, metastatic squamous cell carcinoma of the head and neck. Oral oncology. 2017;67:61–9. [PubMed: 28351582]
5. Huang KK, Jang KW, Kim S, Kim HS, Kim SM, Kwon HJ, et al. Exome sequencing reveals recurrent REV3L mutations in cisplatin-resistant squamous cell carcinoma of head and neck. Sci Rep. 2016;6:19552. [PubMed: 26790612]
6. Mandal R, Senbabaoglu Y, Desrichard A, Havel JJ, Dalin MG, Riaz N, et al. The head and neck cancer immune landscape and its immunotherapeutic implications. JCI Insight. 2016;1(17):e89829. [PubMed: 27777979]
7. Ribas A. Adaptive Immune Resistance: How Cancer Protects from Immune Attack. Cancer Discov. 2015;5(9):915–9. [PubMed: 26272491]
8. Pardoll DM. The blockade of immune checkpoints in cancer immunotherapy. Nat Rev Cancer. 2012;12(4):252–64. [PubMed: 22437870]
9. Gao J, Shi LZ, Zhao H, Chen J, Xiong L, He Q, et al. Loss of IFN-gamma Pathway Genes in Tumor Cells as a Mechanism of Resistance to Anti-CTLA-4 Therapy. Cell. 2016;167(2):397–404 e9. [PubMed: 27667683]
10. Garcia-Lora A, Algarra I, and Garrido F. MHC class I antigens, immune surveillance, and tumor immune escape. J Cell Physiol. 2003;195(3):346–55. [PubMed: 12704644]
11. Marincola FM, Jaffee EM, Hicklin DJ, and Ferrone S. Escape of human solid tumors from T-cell recognition: molecular mechanisms and functional significance. Adv Immunol. 2000;74:181–273. [PubMed: 10605607]
12. Chowell D, Morris LGT, Grigg CM, Weber JK, Samstein RM, Makarov V, et al. Patient HLA class I genotype influences cancer response to checkpoint blockade immunotherapy. Science. 2018;359(6375):582–7. [PubMed: 29217585]
13. Ferris RL, Whiteside TL, and Ferrone S. Immune escape associated with functional defects in antigen-processing machinery in head and neck cancer. Clin Cancer Res. 2006;12(13):3890–5. [PubMed: 16818683]
14. Concha-Benavente F, Srivastava R, Ferrone S, and Ferris RL. Immunological and clinical significance of HLA class I antigen processing machinery component defects in malignant cells. Oral Oncol. 2016;58:52–8. [PubMed: 27264839]
15. Forster MD, and Devlin MJ. Immune Checkpoint Inhibition in Head and Neck Cancer. Front Oncol. 2018;8:310. [PubMed: 30211111]
16. Ferris RL. Immunology and Immunotherapy of Head and Neck Cancer. J Clin Oncol. 2015;33(29):3293–304. [PubMed: 26351330]

17. Cancer Genome Atlas N. Comprehensive genomic characterization of head and neck squamous cell carcinomas. Nature. 2015;517(7536):576–82. [PubMed: 25631445]
18. Cao R, Wang L, Wang H, Xia L, Erdjument-Bromage H, Tempst P, et al. Role of histone H3 lysine 27 methylation in Polycomb-group silencing. Science. 2002;298(5595):1039–43. [PubMed: 12351676]
19. Kim KH, and Roberts CW. Targeting EZH2 in cancer. Nat Med. 2016;22(2):128–34. [PubMed: 26845405]
20. Peng D, Kryczek I, Nagarsheth N, Zhao L, Wei S, Wang W, et al. Epigenetic silencing of TH1-type chemokines shapes tumour immunity and immunotherapy. Nature. 2015;527(7577):249–53. [PubMed: 26503055]
21. Kugelberg E. Tumour immunology: Reducing silence to improve therapy. Nat Rev Immunol. 2015;15(12):730.
22. Wang D, Quiros J, Mahuron K, Pai CC, Ranzani V, Young A, et al. Targeting EZH2 Reprograms Intratumoral Regulatory T Cells to Enhance Cancer Immunity. Cell Rep. 2018;23(11):3262–74. [PubMed: 29898397]
23. Goswami S, Apostolou I, Zhang J, Skepner J, Anandhan S, Zhang X, et al. Modulation of EZH2 expression in T cells improves efficacy of anti-CTLA-4 therapy. J Clin Invest. 2018;128(9):3813–8. [PubMed: 29905573]
24. Zingg D, Arenas-Ramirez N, Sahin D, Rosalia RA, Antunes AT, Haeusel J, et al. The Histone Methyltransferase Ezh2 Controls Mechanisms of Adaptive Resistance to Tumor Immunotherapy. Cell Rep. 2017;20(4):854–67. [PubMed: 28746871]
25. Bugide S, Green MR, and Wajapeyee N. Inhibition of Enhancer of zeste homolog 2 (EZH2) induces natural killer cell-mediated eradication of hepatocellular carcinoma cells. Proc Natl Acad Sci U S A. 2018;115(15):E3509–E18. [PubMed: 29581297]
26. Ennishi D, Takata K, Beguelin W, Duns G, Mottok A, Farinha P, et al. Molecular and Genetic Characterization of MHC Deficiency Identifies EZH2 as Therapeutic Target for Enhancing Immune Recognition. Cancer Discov. 2019.
27. Judd NP, Winkler AE, Murillo-Sauca O, Brotman JJ, Law JH, Lewis JS Jr., et al. ERK1/2 regulation of CD44 modulates oral cancer aggressiveness. Cancer Res. 2012;72(1):365–74. [PubMed: 22086849]
28. Campbell JD, Yau C, Bowlby R, Liu Y, Brennan K, Fan H, et al. Genomic, Pathway Network, and Immunologic Features Distinguishing Squamous Carcinomas. Cell Rep. 2018;23(1):194–212 e6. [PubMed: 29617660]
29. McCabe MT, Ott HM, Ganji G, Korenchuk S, Thompson C, Van Aller GS, et al. EZH2 inhibition as a therapeutic strategy for lymphoma with EZH2-activating mutations. Nature. 2012;492(7427):108–12. [PubMed: 23051747]
30. Knutson SK, Kawano S, Minoshima Y, Warholic NM, Huang KC, Xiao Y, et al. Selective inhibition of EZH2 by EPZ-6438 leads to potent antitumor activity in EZH2-mutant non-Hodgkin lymphoma. Mol Cancer Ther. 2014;13(4):842–54. [PubMed: 24563539]
31. Zolkind P, Przybylski D, Marjanovic N, Nguyen L, Lin T, Johanns T, et al. Cancer immunogenomic approach to neoantigen discovery in a checkpoint blockade responsive murine model of oral cavity squamous cell carcinoma. Oncotarget. 2018;9(3):4109–19. [PubMed: 29423108]
32. Zingg D, Debbache J, Schaefer SM, Tuncer E, Frommel SC, Cheng P, et al. The epigenetic modifier EZH2 controls melanoma growth and metastasis through silencing of distinct tumour suppressors. Nat Commun. 2015;6:6051. [PubMed: 25609585]
33. Jones BA, Varambally S, and Arend RC. Histone Methyltransferase EZH2: A Therapeutic Target for Ovarian Cancer. Mol Cancer Ther. 2018;17(3):591–602. [PubMed: 29726819]
34. Lue JK, and Amengual JE. Emerging EZH2 Inhibitors and Their Application in Lymphoma. Curr Hematol Malig Rep. 2018;13(5):369–82. [PubMed: 30112706]
35. Nienstedt JC, Schroeder C, Clauditz T, Simon R, Sauter G, Muenscher A, et al. EZH2 overexpression in head and neck cancer is related to lymph node metastasis. J Oral Pathol Med. 2018;47(3):240–5. [PubMed: 29285811]

36. Mochizuki D, Misawa Y, Kawasaki H, Imai A, Endo S, Mima M, et al. Aberrant Epigenetic Regulation in Head and Neck Cancer Due to Distinct EZH2 Overexpression and DNA Hypermethylation. Int J Mol Sci. 2018;19(12).

37. Chang JW, Gwak SY, Shim GA, Liu L, Lim YC, Kim JM, et al. EZH2 is associated with poor prognosis in head-and-neck squamous cell carcinoma via regulating the epithelial-to-mesenchymal transition and chemosensitivity. Oral Oncol. 2016;52:66–74. [PubMed: 26604082]

38. Gannon OM, Merida de Long L, Endo-Munoz L, Hazar-Rethinam M, and Saunders NA. Dysregulation of the repressive H3K27 trimethylation mark in head and neck squamous cell carcinoma contributes to dysregulated squamous differentiation. Clin Cancer Res. 2013;19(2): 428–41. [PubMed: 23186778]

39. Pfirschke C, Siwicki M, Liao HW, and Pittet MJ. Tumor Microenvironment: No Effector T Cells without Dendritic Cells. Cancer Cell. 2017;31(5):614–5. [PubMed: 28486102]

40. Christensen JE, de Lemos C, Moos T, Christensen JP, and Thomsen AR. CXCL10 is the key ligand for CXCR3 on CD8+ effector T cells involved in immune surveillance of the lymphocytic choriomeningitis virus-infected central nervous system. J Immunol. 2006;176(7):4235–43. [PubMed: 16547260]

41. Pan D, Kobayashi A, Jiang P, Ferrari de Andrade L, Tay RE, Luoma AM, et al. A major chromatin regulator determines resistance of tumor cells to T cell-mediated killing. Science. 2018;359(6377): 770–5. [PubMed: 29301958]

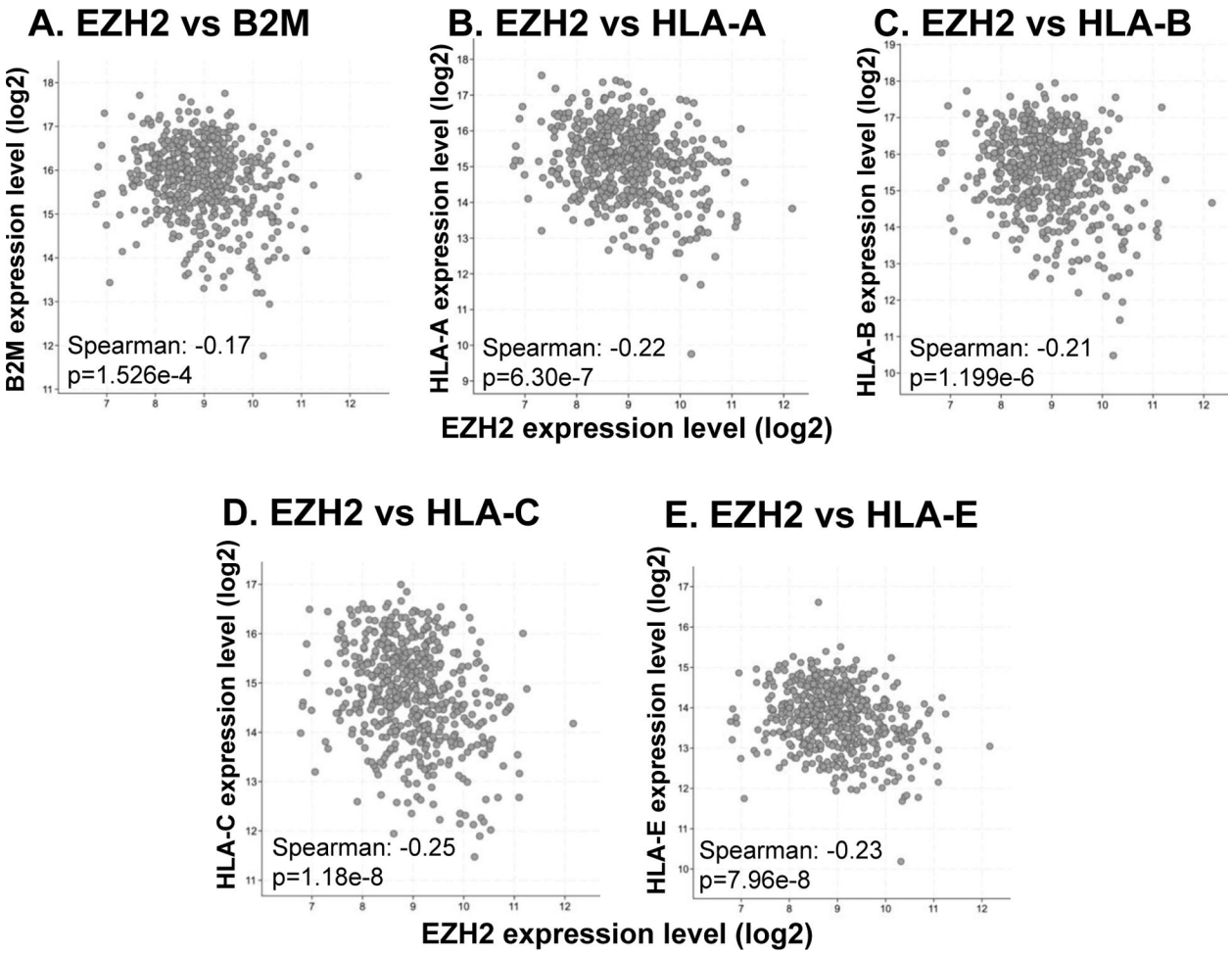

Figure 1. Expression of EZH2 is negatively correlated with major antigen presentation molecules in TCGA head and neck squamous carcinoma data sets.

Correlation between EZH2 and (A) B2M, (B) HLA-A, (C) HLA-B, (D) HLA-C, (E) HLA-E transcripts from 522 HPV-negative head and neck squamous carcinoma samples in TCGA.

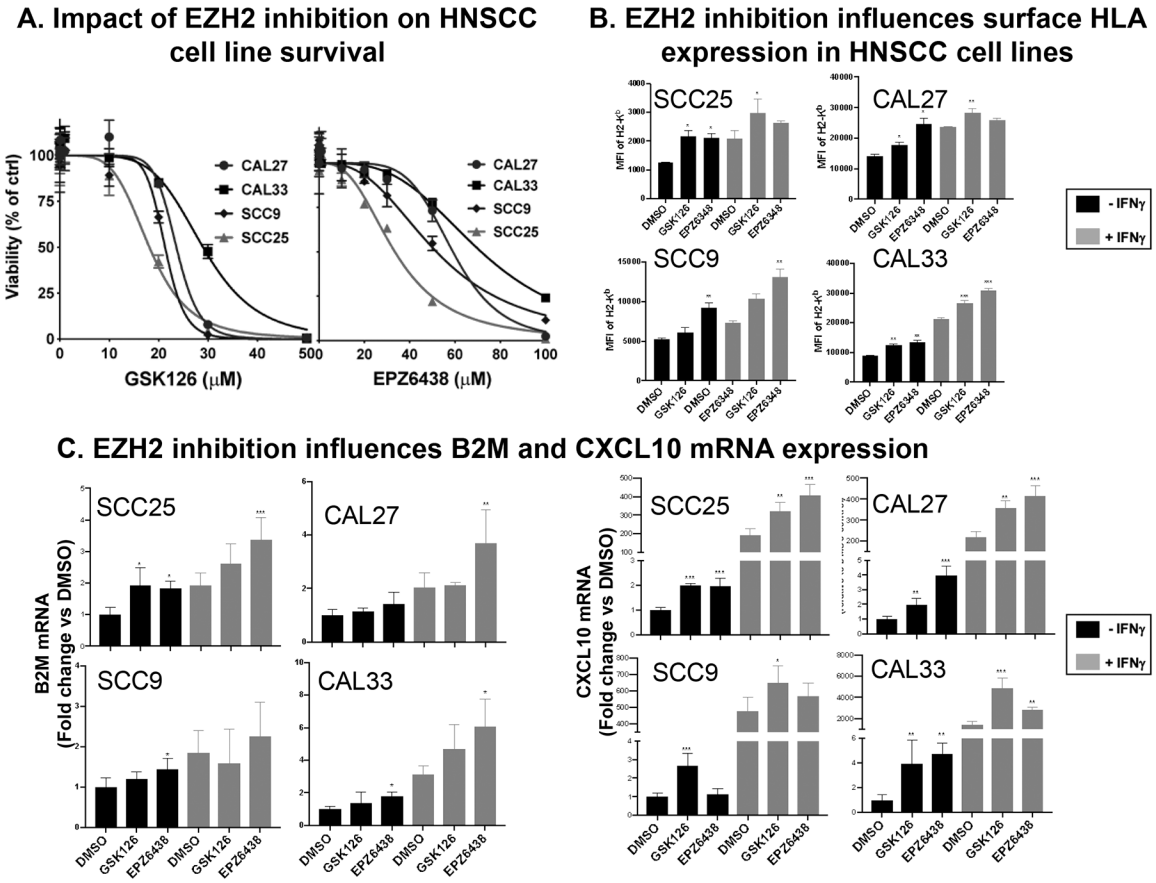

Figure 2. EZH2 inhibition enhances antigen presentation and Th1-type chemokine expression levels in human HNSCC lines.

A. SCC9, SCC25, CAL27, and CAL33 were treated with increasing concentrations of GSK126 or EPZ6348 (1 nM-100 μM) for 72 hours to test assess impact on cell viability. B. Human HNSCC cells were treated with GSK126 (10 μM), EPZ6438 (10 μM), or DMSO as control for 72 hours. IFNγ was added in the last 24 hours of drug incubation for all assays shown. HLA cell surface protein levels were measured by flow cytometry. The data are representative of 2 independent experiments. C. B2M and CXCL10 mRNA expression levels were quantified by qRT-PCR. Relative mRNA levels were normalized to GAPDH. *P<0.05, **P<0.01, ***P<0.001. Significance was calculated by one-way ANOVA. Data are shown as Mean± SD.

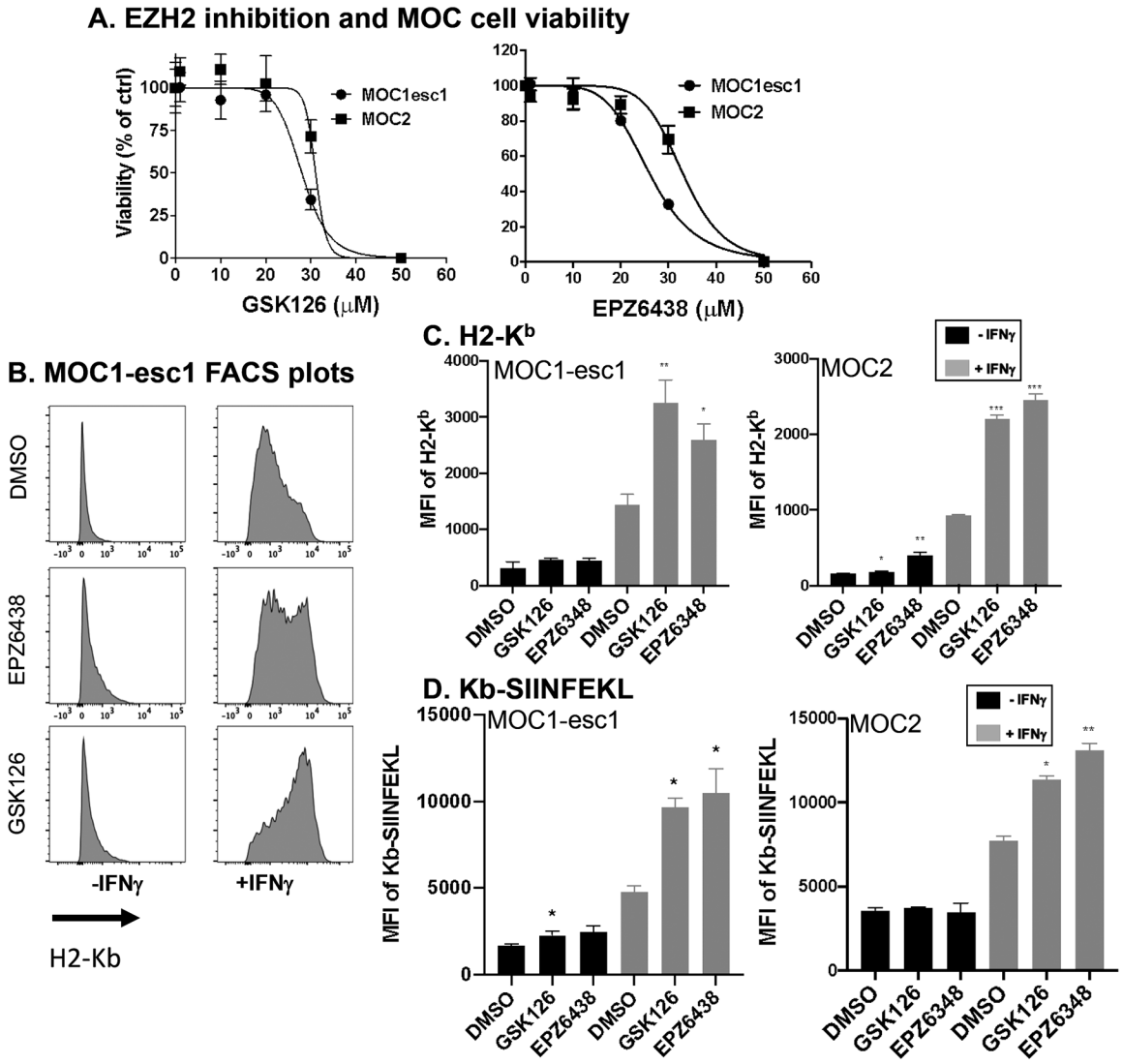

Figure 3. EZH2 inhibition upregulates MHC class I antigen presentation in anti-PD-1 resistant mouse HNSCC cells.

A. MOC1-esc1 and MOC2 cells were incubated with increasing concentrations of GSK126 or EPZ6348 (1 nM-100 μM) for 72 hours to test assess impact on cell viability. B. Representative histogram plots of H2-K^b cell surface expression levels after treatment of GSK126 (10 μM), EPZ6348 (10 μM), or DMSO in MOC1-esc1 cells. C. Quantification of H2-K^b cell surface expression levels in MOC1-esc1 and MOC2. The data are representative of 2 independent experiments. D. MOC1-esc1 cells were treated by GSK126, EPZ6348, or DMSO for 72 hours in the presence of IFNγ. Subsequently cells were incubated with 1μM of OVA peptide at 37 degree for 2 hours. Cells were stained for OVA-Kb to assess the antigen presentation capacity using flow cytometry. The data are representative of 2 independent experiments. **P*<0.05, ***P*<0.01, ****P*<0.001. Significance was calculated by one-way ANOVA. Data are shown as Mean± SD.

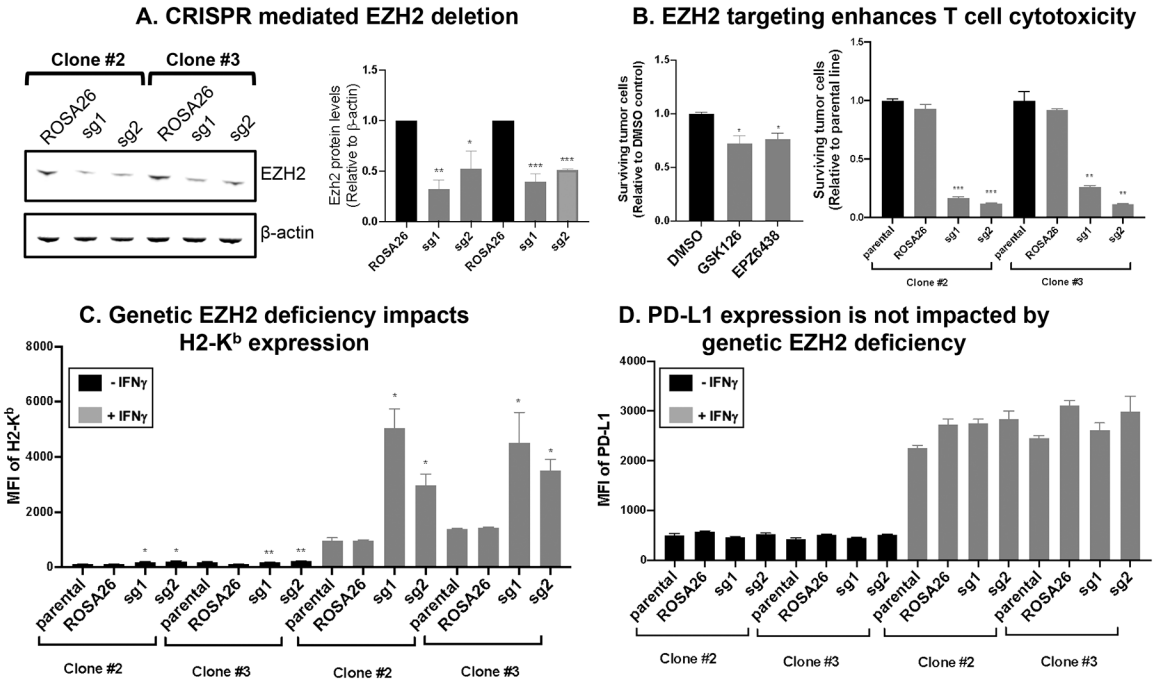

Figure 4. Pharmacological inhibition and genetic ablation of EZH2 in tumor cells enhance T-cell mediated killing in vitro.

A. Two CAS9 expressing MOC1-esc1 cell clones, clone #2 and #3 were transduced with 2 independent GFP tagged gRNAs specific for EZH2 genomic editing or ROSA26 control. GFP positive cells were sorted as edited cells. Cell lysates were probed for EZH2 expression with b-actin loading control. The data are representative of 2 independent experiments. **B.** Tumor: T cell co-culture assay in left panel with GSK126 or EZP6438 inhibition and right panel with EZH2 CRISPR lines. For pharmacological inhibition, MOC1-esc1 cells were treated with 10 μM of GSK126, EPZ6438, or DMSO for 72 hours in the presence of IFNγ. Cells were pulsed with SIINFEKL peptide (0.02 nM, for 2 hours at 37 degrees). In vitro activated and expanded OT-1 T cells were plated with antigen pulsed tumor cells at an E:T ratio of 0.5. After 24 hours of coculture, surviving tumor cells were counted by flow cytometry. Right panel shows co-culture assay with EZH2 deficient cell lines. The data are representative of 2 independent experiments. **C, D**. Cell surface H2-K^b and PD-L1 expression levels were measured in EZH2 edited and the control lines. The data are representative of 2 independent experiments. *P<0.05, **P<0.01, ***P<0.001. Significance was calculated by Student's t test and one-way ANOVA. Data are shown as Mean± SD.

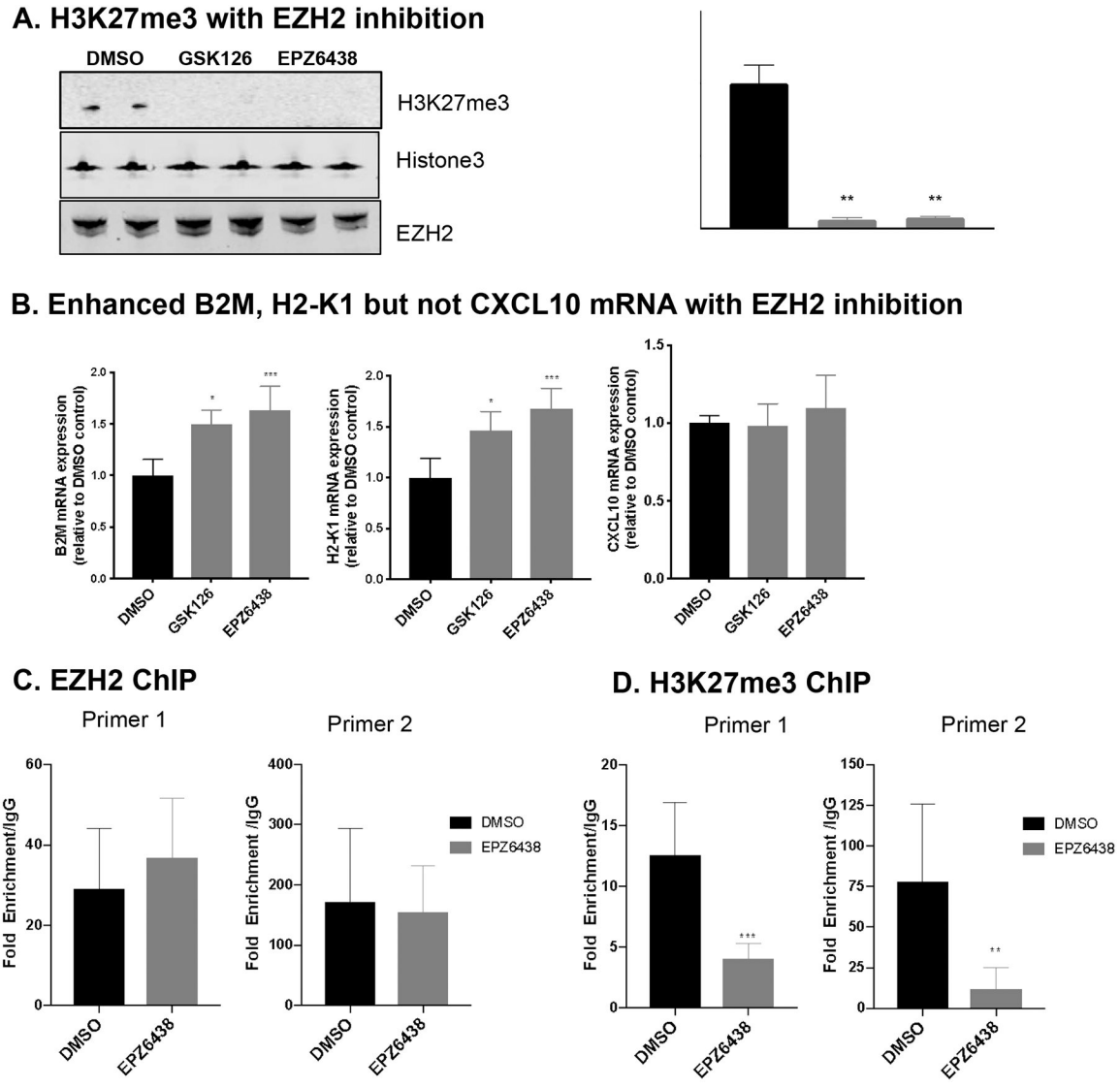

Figure 5. EZH2 is a repressor of antigen presentation by regulating the enrichment of H3K27me3 on the promoter regions of B2M.

A. MOC1-esc1 cells were treated with GSK126 (10 μM), EPZ6438 (10 μM), or DMSO as control for 72 hours. H3K27me3 and EZH2 protein levels were determined by western blot. Total H3 was used as loading control. **B.** The mRNA expression levels of B2M, H2-K1, and CXCL10 were measured by qRT-PCR in MOC1-esc1 cells treated with EZH2 inhibitors and IFNγ. Relative mRNA levels were normalized to GAPDH. **C, D.** Chromatin immunoprecipitation (CHIP) for EZH2, H3K27me3, and IgG, and subsequent qPCR in B2M promoter using two independent primer sets. **P*<0.05, ***P*<0.01, ****P*<0.001. Significance was calculated by one-way ANOVA and Student's *t* test. Data are shown as Mean± SD.

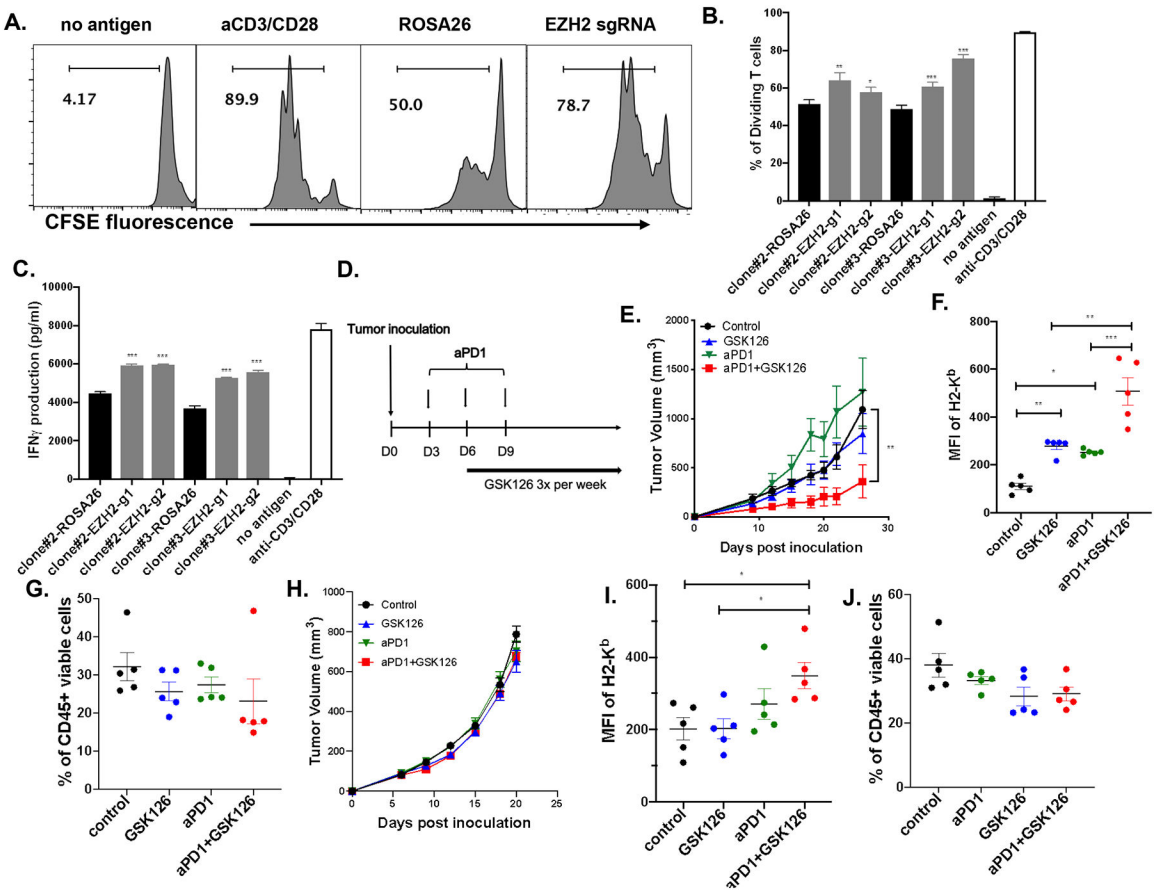

Figure 6. Combinatorial therapy of GSK126 and anti-PD-1 suppresses MOC1-esc1 tumor progression.

A. Representative histogram plots showing T cell proliferation in experimental and control conditions. IFNγ pre-treated EZH2 edited and control cells were pulsed with 1 μM SIINFEKL peptide at 37 degree for 2 hours and co-cultured with CFSE labeled naïve OT-1 cells at an E:T ratio of 10:1 for 72 hours. T cell proliferation was analyzed by flow cytometry. No Antigen condition represents CFSE labeled T cells without tumor cells. The data are representative of 2 independent experiments and shown as Mean ± SD. **B.** Quantitative analysis of proliferating T cells between indicated conditions. **C.** IFNγ concentration was measured in the co-culture media by ELISA. **D.** Schematic of experimental design for in vivo combination therapy. **E.** C57BL/6 mice (n=4) inoculated subcutaneously with MOC1-esc1 (10^6) cells. Anti-PD-1 antibody was IP injected on Day 3, 6, and 9 post-inoculation. GSK126 was IP injected 3 times a week starting from Day 6 post-inoculation and tumor growth was monitored. The data are representative of 2 independent experiments and shown as Mean± SEM. **F, G**. Tumors were harvested on D12 post-inoculation. H2-Kb on tumor cell surface (CD45 negative) and percentage of CD45+ cells in each indicated condition were analyzed by flow cytometry. **H.** The effect of indicated treatment on MOC2 tumor progression (n=10). **I, J**: MOC2 tumors were harvested on D22 post-inoculation (n=5). H2-Kb on tumor cell surface (CD45 negative) and percentage of CD45+ cells in each indicated condition were analyzed by flow cytometry.

*P<0.05, **P<0.01, ***P<0.001. Significance was calculated by one-way ANOVA and 2-way ANOVA.